Journal of Medical Imaging

MedicalImaging.SPIEDigitalLibrary.org

# High spatial resolution diffusion weighted imaging on clinical 3 T MRI scanners using multislab spiral acquisitions

Joseph L. Holtrop
Bradley P. Sutton

SPIE.

Joseph L. Holtrop, Bradley P. Sutton, "High spatial resolution diffusion weighted imaging on clinical 3 T MRI scanners using multislab spiral acquisitions," *J. Med. Imag.* **3**(2), 023501 (2016), doi: 10.1117/1.JMI.3.2.023501.

# High spatial resolution diffusion weighted imaging on clinical 3 T MRI scanners using multislab spiral acquisitions

**Joseph L. Holtrop**[a,b,*] **and Bradley P. Sutton**[a,b]
[a]University of Illinois at Urbana-Champaign, Department of Bioengineering, 1270 Digital Computer Laboratory, MC-278, Urbana, Illinois 61801, United States
[b]University of Illinois at Urbana-Champaign, Beckman Institute for Advanced Science and Technology, 405 North Mathews, MC-251, Urbana, Illinois 61801, United States

**Abstract.** A diffusion weighted imaging (DWI) approach that is signal-to-noise ratio (SNR) efficient and can be applied to achieve sub-mm resolutions on clinical 3 T systems was developed. The sequence combined a multislab, multishot pulsed gradient spin echo diffusion scheme with spiral readouts for imaging data and navigators. Long data readouts were used to keep the number of shots, and hence total imaging time, for the three-dimensional acquisition short. Image quality was maintained by incorporating a field-inhomogeneity-corrected image reconstruction to remove distortions associated with long data readouts. Additionally, multiple shots were required for the high-resolution images, necessitating motion induced phase correction through the use of efficiently integrated navigator data. The proposed approach is compared with two-dimensional (2-D) acquisitions that use either a spiral or a typical echo-planar imaging (EPI) acquisition to demonstrate the improved SNR efficiency. The proposed technique provided 71% higher SNR efficiency than the standard 2-D EPI approach. The adaptability of the technique to achieve high spatial resolutions is demonstrated by acquiring diffusion tensor imaging data sets with isotropic resolutions of 1.25 and 0.8 mm. The proposed approach allows for SNR-efficient sub-mm acquisitions of DWI data on clinical 3 T systems.  [DOI: 10.1117/1.JMI.3.2.023501]

Keywords: diffusion MRI; spiral MRI; multishot diffusion imaging.

Paper 15244LRR received Dec. 15, 2015; accepted for publication Mar. 14, 2016; published online Apr. 12, 2016.

## 1 Introduction

There is significant interest in improving the quality and spatial resolution of diffusion weighted imaging (DWI) data. Both researchers and clinicians want data that is higher spatial resolution, has less magnetic susceptibility distortions, and remains high in signal-to-noise ratio (SNR). Achieving these features in DWI has been limited due to excessive scan time and distortions associated with long data readouts. Several recent approaches to address the challenges of SNR and artifacts have included specialized scanning hardware, pulse sequence modifications, and image reconstruction advances.[1–4]

While many of the recent advances have focused on specialized hardware, the proposed approach will enable high resolution imaging on any hardware configuration. Achieving sufficient SNR for a high-resolution diffusion scan relies on minimizing the echo time (TE) and operating at an SNR-optimal repetition time (TR). In addition to this acquisition optimization, an image reconstruction technique is required that is capable of modeling phase errors associated with multishot data while reducing distortions caused by long data readouts which are required for reasonable scan times at higher resolutions. Furthermore, the proposed sequence incorporates an efficient navigator strategy to reduce the total time required to acquire data for each shot, enabling more usable imaging data to be collected in the same amount of scan time.

In terms of minimizing TE, the pulsed gradient spin echo (PGSE) sequence[5] allows for the shortest diffusion encoding preparation time. However, being able to achieve a short echo time using PGSE encoding is dependent on the k-space trajectory being used. Center out k-space trajectories, such as spiral, are able to achieve the shortest echo times. Echo-planar imaging (EPI) trajectories have the potential to incur large TE penalties, especially as the spatial resolution of the scan increases. However, some of this TE penalty can be reduced by using parallel imaging combined with a partial Fourier acquisition. By using center-out k-space trajectories with PGSE diffusion encoding, a reduction of 10 to 15 ms in TE could be expected on most clinical systems when compared with trajectories that do not sample the center of k-space early in the readout. The gain due to TE by switching to center-out k-space trajectories is not as significant in the commonly used twice refocused spin echo (TRSE) EPI acquisition[6] that is frequently used on 3 T clinical hardware, however, this technique pays a penalty in TE as its diffusion encoding is not as efficient. The switch to PGSE has the potential to significantly increase artifacts due to eddy currents on some hardware, but recent processing tools, such as the "eddy" tool in FMRIB software library (FSL),[7] have been able to greatly reduce these concerns, especially in combination with advances in hardware[8] that reduce the impact of eddy currents.

In this work, a multishot, three-dimensional (3-D) multislab PGSE sequence is used to achieve sub-mm isotropic, whole

*Address all correspondence to: Joseph L. Holtrop, E-mail: holtrop1@illinois.edu

2329-4302/2016/$25.00 © 2016 SPIE

brain acquisitions for diffusion weighted imaging. The sequence features a short spiral-in navigator for motion correction followed by a longer spiral-out readout for imaging data acquisition with several optimizations to improve the SNR efficiency. SNR efficiency is defined as the SNR of an image divided by the square root of the scan time to acquire data for the image. The definition is motivated by the square root improvement in SNR from simple averaging. The proposed acquisition enables SNR efficiency benefits from: shorter echo times from the spiral acquisitions, optimized TR for $T_1$ recovery and signal averaging tradeoffs, and optimized data readout durations from the multishot spiral. An iterative image reconstruction scheme is used that is able to correct for distortions that accompany the long data readouts. Using long data readouts increases the SNR efficiency of the acquisition by acquiring more of the imaging k-space per time-consuming diffusion encoding module.[9] The SNR benefits of the proposed method will be shown at resolutions commonly used for single shot DWI. Finally, the ability of the technique to achieve even higher spatial resolution and sub-mm acquisitions will be shown.

## 2 Materials and Methods

### 2.1 *Three-Dimensional k-Space Encoding for Optimal Repetition Time*

The choice of optimal TR is influenced primarily by the $T_1$ of the object as having a short TR results in signal loss due to incomplete $T_1$ recovery and having a long TR reduces SNR efficiency. Balancing how often data is collected for averaging and the $T_1$ recovery, the optimal TR is ~1.5 seconds[2] using a $T_1$ of 1.1 s for white matter at 3 T.[10] In order to maintain whole-brain coverage with such a short TR, multiple slices must be grouped into 3-D slabs. However, for multislab acquisitions the SNR-efficient TR increases to 2 to 3 s when imperfections in RF excitation profiles are considered.[11] By switching to a 3-D excitation scheme, which samples data for multiple slices in a 3-D volume, the SNR efficiency can be increased by 50% or more in the same total imaging time compared with a standard two-dimensional (2-D) acquisition when imaging a large number of slices.[2,9,11,12]

### 2.2 *Spiral Readouts for Short Echo Time*

The spiral trajectory is a commonly used non-Cartesian trajectory due to its ability to efficiently cover k-space by better leveraging gradient hardware limitations than the EPI trajectory. A spiral trajectory also has the property of being able to sample the center of k-space at the start of the readout, this can allow for significantly shorter TEs to be achieved. This is in contrast to commonly used EPI acquisitions which suffer from expanding echo times when the spatial resolution of the acquisition is increased. The spiral trajectory is also extremely flexible in its design allowing an arbitrary number of shots to be designed to cover k-space in multiple acquisitions. This allows for fine control over the amount of undersampling per shot and the readout duration, to limit susceptibility distortions and $T_2$*-induced blurring. Long readouts are desirable as they will limit the total number of shots required to form an image; however, longer readouts come with increased magnetic susceptibility-induced distortion that must be addressed during image reconstruction. To achieve 3-D encoding with spiral, the stack of spirals k-space trajectory is used in the current work, but other choices are possible.[13,14]

### 2.3 *Navigation for Multishot Diffusion*

At high resolutions, a multishot acquisition becomes necessary to limit the duration of the long data readouts to limit the $T_2$* blurring and image distortions. In DWI, using multiple shots leads to motion-induced phase errors (MPE) due to different shots having differences in small amounts of motion during diffusion encoding.[15] These phase errors lead to artifacts and signal cancellations in the reconstructed image if not corrected. A wide variety of techniques have been developed to handle these errors.[16–24] In addition to subject motion during DWI, these phase errors can be caused by cardiac pulsation or other physiological motions, which may result in nonlinear MPE. The sequence in this work uses a spiral-in readout to acquire a low resolution 2-D navigator image which allows it to be used with most navigator-based motion-correction methods. As long as the resolution of the navigator allows for it to capture the spatial variations of the MPE, the proposed sequence will be scalable to higher imaging resolutions without being limited by the resolution of the navigator. The 2-D navigator for a 3-D slab assumes that the spatial variation of MPE in the slice direction is small, which has been shown to be accurate as long as the slabs are thin.[2]

### 2.4 *Proposed Pulse Sequence*

The proposed acquisition sequence is designed to achieve a high SNR efficiency. The acquisition uses a standard PGSE[5] approach for encoding diffusion due to its efficient diffusion

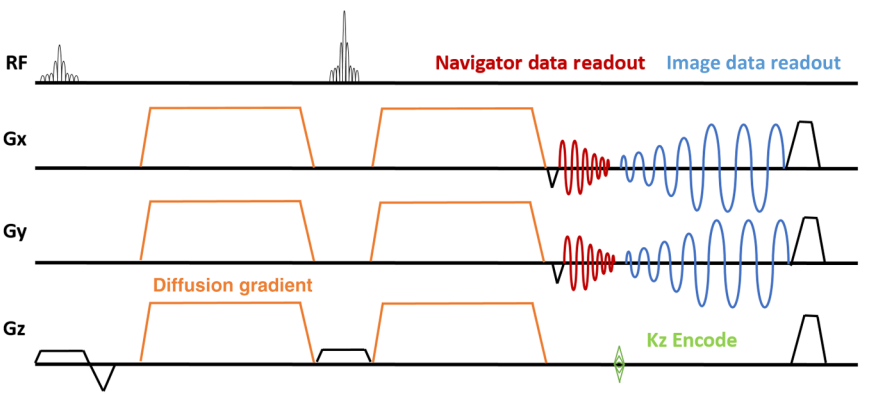


**Fig. 1** Pulse sequence diagram for the proposed SNR optimized 3-D multislab, multishot navigated DWI sequence.

encoding and a 3-D multislab approach due to its ability to balance sampling time for a slice with adequate $T_1$ recovery. The use of spiral readouts also enable the short echo time provided by the PGSE scheme to be utilized, enabling higher SNR by shortening the TE. The pulse sequence used to achieve this is shown in Fig. 1. Additionally, a spectrally selective lipid excitation and spoiler gradient is used for lipid suppression (not shown), free induction decay crusher gradients are used for low $b$-values, and gradient spoiling is used after the spiral readout.

A short spiral-in navigator is placed immediately after the second diffusion-encoding gradient followed by a kz phase encoding gradient and then a spiral readout for imaging data. For a PGSE sequence, this spiral-in navigator does not add any time to the imaging sequence as long as it is shorter than the slice select rewinder plus one half the excitation pulse duration minus the duration of the kz encode. The placement of the navigator directly before the imaging readout instead of after a second refocusing pulse is beneficial because it does not impact scan time efficiency. A spiral navigator with a $40 \times 40$ matrix size acquired with a parallel imaging factor $R = 2$ is used for navigation.

In order to minimize artifacts associated with imperfections in 3-D slab excitation, several considerations were made. First, we used relatively long (10 ms) RF pulses that were designed using the Shinnar–Le Roux procedure[25] to result in sharp transition widths. Additionally, the number of slices in a slab was kept low in order to decrease the amount of signal loss that can sometimes be observed at edge slices. The slabs were also excited in an interleaved manner to reduce interactions between adjacent slabs. Finally, a TR is used that is slightly longer than the $T_1$-optimal TR to enable further relaxation between adjacent slabs.

### 2.5 *Image Reconstruction*

An iterative, model-based image reconstruction scheme is used to allow modeling of non-Cartesian spiral readouts, nonlinear MPE,[22] parallel imaging using sensitivity encoding,[26] and correction for magnetic susceptibility-induced image distortions.[27] The magnetic field inhomogeneity correction enables the use of longer readouts, reducing the total number of shots, with their diffusion encoding overhead, leading to a higher SNR efficiency.[28]

### 2.6 *In Vivo Data*

In vivo data were collected on Siemens 3 T Trio scanner using a 32-channel head coil. Scanning was done under local institutional review board approval with all subjects giving written consent before participating. To compare the SNR achievable with the optimized, 3-D multislab sequence, several data sets using EPI and spiral with a variety of imaging parameters were obtained, see Table 1 for a description of the parameters of these acquisitions. First, a standard spatial resolution of 2 mm isotropic was targeted, collecting DWI data with a 2-D acquisition with both single-shot EPI (referred to as "2-D_EPI") and spiral readouts (referred to as "2-D_spiral"). The 2-D_EPI acquisition was chosen as a basis of comparison as it is the most commonly used acquisition on clinical MRI scanners at 2 mm spatial resolution. The proposed 3-D multislab acquisition with 2 mm isotropic resolution (referred to as "3-D_spiral") was acquired with a single in-plane shot for each kz encoding in order to match readout duration for single shot imaging with the 2-D_spiral protocol. For all of these acquisitions, the same FOV and slice coverage were used with the minimum TE and TR possible for each technique. Notably, these acquisitions all require the exact same number of excitations to do the imaging as all are single-shot in a kz plane or single-shot within a 2-D slice. A high resolution $T_1$-weighted MPRAGE (TE: 2.3 ms, TR: 1900 ms, TI: 900 ms, FOV: $230 \times 172 \times 230$ mm, matrix $256 \times 192 \times 256$) was acquired. Additionally, reference images with different echo times were acquired for field map estimation[29] to enable field inhomogeneity correction[27] and to estimate the coil sensitivity map.[26] This scan utilized an asymmetric spin echo, spin echo TE of 17 ms, gradient echo TE was 1 ms delayed, matrix size: $120 \times 120$, FOV: $240 \times 240$ mm, slices: 40, slice thickness: 3 mm, TR: 1800 ms.

SNR measurements were derived by taking the temporal mean divided by the temporal standard deviation from 25 repeats of each measurement for a single diffusion encoding direction. A white matter mask was obtained in the subject's

**Table 1** Sequence protocols.

| Name | Sequence | TE (ms) | TR (s) | Total scan time (s) | Resolution/matrix size/coverage | Total shots per image | Readout duration (ms) | Number of images/ diffusion encoding |
|---|---|---|---|---|---|---|---|---|
| 2-D_EPI | TRSE EPI (GRAPPA $R = 3$) | 92 | 9.60 | 480 | 2 mm isotropic $120 \times 120$ 60 slices | 1 | 27 | 25 ($b = 0$) 25 ($b = 1000$) |
| 2-D_spiral | PGSE (spiral $R = 3$) | 73 | 7.26 | 363 | 2 mm isotropic $120 \times 120$ 60 slices | 1 | 20 | 25 ($b = 0$) 25 ($b = 1000$) |
| 3-D_spiral | PGSE (spiral $R = 3$) | 81 | 1.97 | 394 | 2 mm isotropic $120 \times 120 \times 4$ 15 slabs 4 slices/slab | 4 | 20 | 25 ($b = 0$) 25 ($b = 1000$) |
| 3-D_spiral_ HR1 | PGSE (spiral $R = 2$) | 83 | 3.10 | 1190 | 1.25 mm isotropic $192 \times 192 \times 4$ 24 slabs 4 slices/slab | 12 | 29 | 2 ($b = 0$) 30 directions ($b = 1000$) |
| 3-D_spiral_ HR2 | PGSE (spiral $R = 2$) | 80 | 2.00 | 5120 | 0.8 mm isotropic $300 \times 300 \times 20$ 1 slabs 20 slices/slab | 80 | 52 | 2 ($b = 0$) 30 direction ($b = 1000$) |
| 2-D_EPI_ DTI | TRSE EPI (GRAPPA $R = 2$) | 95 | 2.00 | 64 | 2 mm isotropic $120 \times 120$ 8 slices | 1 | 41 | 2 ($b = 0$) 30 directions ($b = 1000$) |

diffusion tensor imaging (DTI) space by segmenting the MPRAGE image using FMRIB's automatic segmentation tool[30] in FSL[31] and then registering the segmentations to the diffusion weighted images using FLIRT.[32,33] The pixel-wise SNR was then averaged across the mask to create a single image SNR value for each of the acquisitions: 2-D_EPI, 2-D_spiral, and 3-D_spiral. SNR efficiency was calculated by taking the SNR in the image and dividing it by the square root of scan time required to acquire the image.

To demonstrate that the proposed sequence can be used at higher resolutions, a 1.25 mm isotropic (3-D_spiral_HR1) and 0.8 mm isotropic DWI data sets (3-D_spiral_HR2) were acquired with the proposed sequence. A matched coverage 2 mm resolution data set (2-D_epi_DTI) was acquired to compare 0.8 mm to 2 mm resolution. Fractional anisotropy (FA) images were created using DTIFit[34] in FSL. These data acquired 30 different diffusion directions for estimating a diffusion tensor in order to match what is most commonly done at lower resolutions. However, depending on the diffusion model being used it may be possible that other diffusion schemes may be better for estimating a tensor.[35]

## 3 Results

First, we demonstrate the SNR gains from spiral through shorter TE and from the 3-D multislab excitation, compared with a modern 2-D EPI acquisition. Then, the use of the SNR gains to obtain DWI data at higher spatial resolutions is shown.

### 3.1 *Signal-to-Noise Ratio Analysis*

Table 2 provides the parameters for each acquisition protocol along with the theoretical relative SNR efficiency from those protocols, compared with the parameters used in the 2-D EPI acquisition. The "SNR efficiency from TR" is the theoretical change in signal due to changing TR using a standard spin echo recovery equation, assuming the sequences have the same readout and TE. The "SNR ratio from TE" is the amount of signal gained by reducing the TE due to a spiral trajectory assuming the TR and readout are the same between sequences. These equations use white matter values of 1.1 ms for $T_1$ and 69 ms for $T_2$.[10] The SNR ratio for a single image is the theoretical gain in SNR taking into account the TE, TR, and readout durations, which includes the gains in SNR due to a 3-D acquisition. The SNR efficiency additionally takes into account the time it takes to acquire an image, normalizing the image SNR by the square root of the acquisition time.

Table 3 summarizes the SNR measurements from 5 subjects across the 2-D_EPI, 2-D_spiral, and 3-D_spiral acquisitions that all had 2 mm isotropic resolution. Table 3 also gives the estimated SNR efficiency increase of 53% from the shorter TE and TR associated with spiral by comparing the 2-D_EPI with the 2-D_spiral acquisitions. It also gives the estimated SNR efficiency increase of 71% for the 3-D encoding and spiral acquisition over the 2-D EPI. Figure 2 shows a comparison of the reconstruction of a single slice for the three different acquisitions used for the SNR analysis.

**Table 2** Theoretical differences in SNR and SNR efficiency.

| Name | TE (ms) | TR (s) | Total ADC time (ms) | SNR ratio from TR | SNR ratio from TE | SNR ratio for single image | SNR efficiency ratio |
|---|---|---|---|---|---|---|---|
| 2-D_EPI | 92 | 9.60 | 16.8 | — | — | — | — |
| 2-D_spiral | 73 | 7.26 | 20.0 | 0.99 | 1.32 | 1.44 | 1.65 |
| 3-D_spiral | 81 | 1.97 | 80.0 | 0.83 | 1.17 | 2.11 | 2.33 |

**Table 3** Comparison of SNR and SNR efficiency across 5 subjects (S1 to S5) at $b = 1000$. The percentage increase in SNR and SNR efficiency over the equivalent 2-D EPI acquisition is given at the bottom of the table.

| | 2-D_EPI ($b = 1000$) | 2-D_spiral ($b = 1000$) | 3-D_spiral ($b = 1000$) |
|---|---|---|---|
| S1 | 7.0 | 9.6 | 10.6 |
| S2 | 7.5 | 9.8 | 11.3 |
| S3 | 7.5 | 10.1 | 11.6 |
| S4 | 8.2 | 11.0 | 12.8 |
| S5 | 7.5 | 9.7 | 11.5 |
| Average (±Std) | 7.5 (0.4) | 10.0 (0.6) | 11.6 (0.8) |
| SNR ratio from 2-D_EPI | — | 1.33 | 1.55 |
| SNR efficiency ratio from 2-D_EPI | — | 1.53 | 1.71 |

### 3.2 *In-Vivo DTI Images*

The ability of the proposed method to acquire multiple direction diffusion data at higher spatial resolution (1.25 mm isotropic) in a reasonable time (19.8 min for 30 direction DTI data) is demonstrated in Fig. 3 using the 3-D_spiral_HR1 data set.

To demonstrate the scalability to higher resolutions, the 3-D multislab sequence was used to acquire a 30-direction data set at a 0.8 mm isotropic resolution (3-D_spiral_HR2). Figure 4 shows the color-coded FA from the 0.8 mm isotropic acquisition. At this increased resolution, partial volume effects of fine white matter structures are greatly reduced.

In order to achieve a short total acquisition time and maintain a high acquisition efficiency, the collection of longer data readouts per diffusion encoding is desired. As previously stated, this results in a tradeoff with magnetic field inhomogeneity induced image distortion. Figure 5 shows the image reconstruction results for a single slice in a 3-D slab with and without field correction from the 3-D_spiral_HR2 acquisition along with type of distortion observed when no motion correction is used. The spiral readout for this imaging data had a relatively long duration of 52 ms. The long data readout results in significant susceptibility-induced distortions in the image, which are radial blurs for spiral acquisitions. Using the magnetic field inhomogeneity corrected image reconstruction, a high-quality image was recovered from the data.

## 4 Discussion

This study demonstrated the feasibility of a multislab 3-D spiral diffusion acquisition to achieve high-resolution DWI (sub-mm isotropic) on a clinical 3 T MRI scanner. The proposed sequence can achieve higher SNR than a standard 2-D EPI acquisition with whole brain coverage at the same spatial resolution and

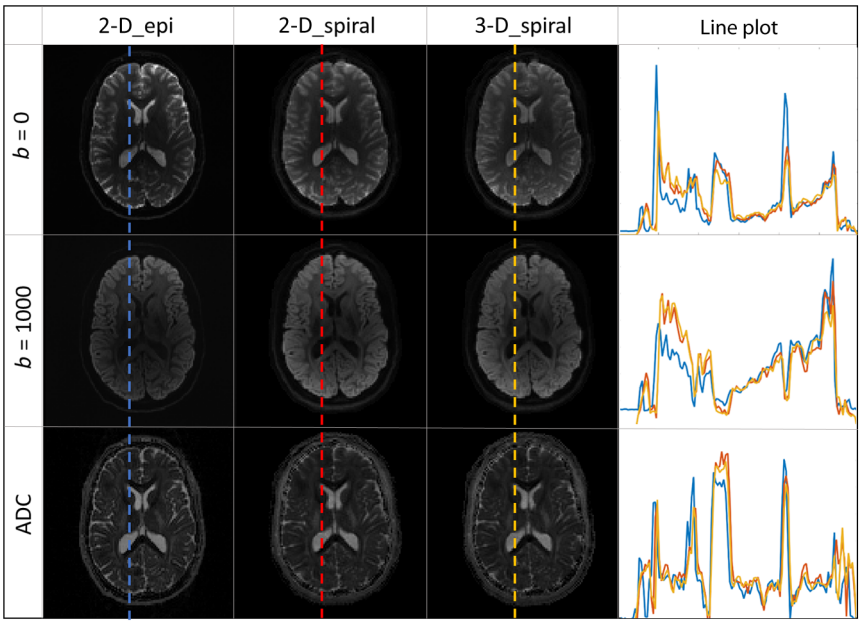


**Fig. 2** Comparison of resulting images for $b = 0$, $b = 1000$, and estimated ADC from the 2-D_EPI, 2-D_spiral, and 3-D_spiral acquisitions for a single slice. A line plot through the image is shown in the right column to more closely look at the differences in the images.

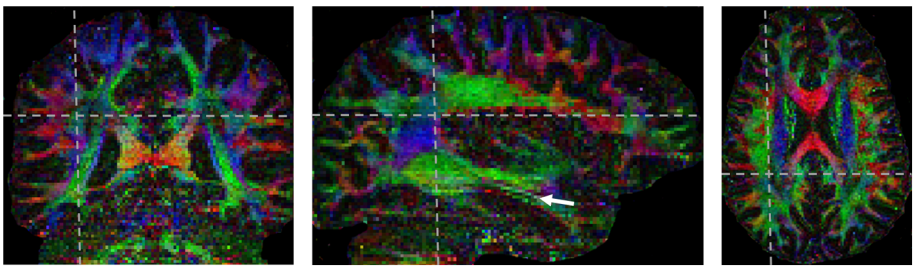

**Fig. 3** 1.25 isotropic FA images from spiral_3-D_HR1 data set. Color-coded FA image, with red left–right, blue inferior–superior, green anterior–posterior. Note the resolved fine white matter structures, such as the hippocampal layers as indicated by the arrow.

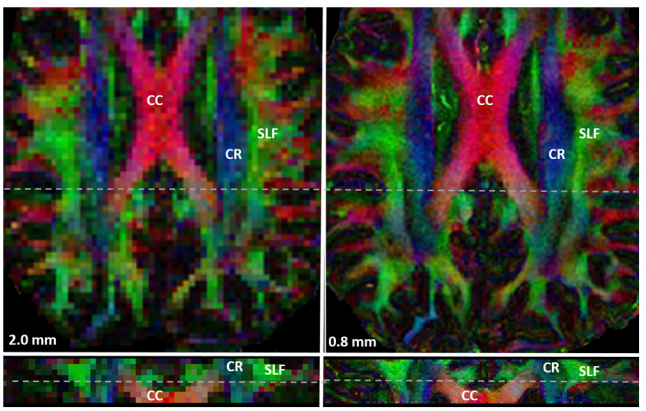


**Fig. 4** Color-coded FA images: (a) 2 mm isotropic and (b) 0.8 mm isotropic. Several commonly studied white matter regions are labeled, including the corpus callosum (CC), corona radiata (CR), and the superior longitudinal fasciculus (SLF). An axial view is shown on top with a coronal view on bottom.

same scan time. The gains in SNR come from using spiral readouts to shorten TE and from the SNR-optimized TR combined with a 3-D multislab acquisition approach. While the spiral readout was chosen for this study, other center out k-space trajectories could also achieve SNR gains due to shorter echo times which are uncoupled from increases in spatial resolution. Additionally by using an iterative, model-based reconstruction scheme, a flexible approach was created capable of using non-Cartesian k-space trajectories, k-space under sampling, and correction for distortions due to long data readouts.

The use of a 3-D multislab spiral acquisition provided SNR efficiency gains over the commonly used 2-D EPI acquisition for the same coverage and without increasing scan time. The 2-D spiral acquisition showed a 53% increase in SNR efficiency over the 2-D EPI acquisition. This is similar to the expected theoretical gain of 65%. For the 3-D spiral acquisition, a 71% increase in SNR efficiency was achieved over the 2-D EPI acquisition. Theoretically a gain of 133% was expected, significantly higher than the measured gain in SNR efficiency. Differences in

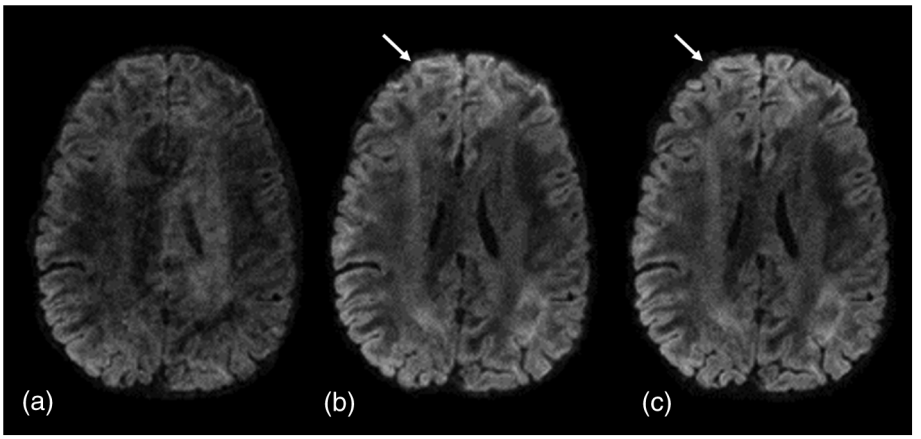


**Fig. 5** 3-D_spiral_HR2 images (0.8 mm isotropic resolution): (a) without MPE correction and without field inhomogeneity correction, (b) with MPE correction and without field inhomogeneity correction, and (c) with MPE correction and with field inhomogeneity correction. The frontal region (indicated by arrows) are the areas that are most impacted by field inhomogeneity in this slice.

SNR for this comparison could be due to decreases in signal at the edge of slabs in the 3-D excitation or from incomplete motion induced phase error correction as the 3-D acquisition uses multiple shots across kz to acquire an imaging volume.

The navigator acquired with the proposed acquisition provided sufficient information to correct for nonlinear motion induced phase errors. Additionally, the location of the navigator allowed for shorter scan times as a second refocusing pulse for a separate navigator was not required.

The technique was successfully applied to achieve much higher resolutions than what are commonly acquired with whole brain coverage on clinical 3 T MRI scanners. The ability to achieve sub-mm isotropic resolutions (sub $\mu$L voxel volume) provides great promise for the field of diffusion neuroimaging. At this resolution partial volume effects are greatly reduced allowing for much better distinctions between fine white and gray matter structures, along with more accurate measures of diffusion properties in these fine structures.

## 5 Conclusion

The proposed technique enables high spatial resolution DWI acquisitions to be acquired, including sub-mm acquisitions, on clinical 3 T hardware. Combining motion-induced phase measurement and correction, 3-D multislab acquisitions, and magnetic field inhomogeneity correction, an acquisition approach was proposed and validated demonstrating significant gains in SNR efficiency over standard approaches. The proposed approach provides a promising technique to study fine white matter fiber structures in complex geometries, reducing partial volume effects.

### *Acknowledgments*

Research reported in this publication was supported by the National Institute of Biomedical Imaging and Bioengineering of the National Institutes of Health under Award Numbers R01EB018107 and R21EB009768. The content is solely the responsibility of the authors and does not necessarily represent the official views of the National Institute of Biomedical Imaging and Bioengineering or the National Institutes of Health. Additional support came from the National Science Foundation under Grant No. 0903622.

### *References*

1. R. Frost et al., "3D multi-slab diffusion-weighted readout-segmented EPI with real-time cardiac-reordered K-space acquisition," *Magn. Reson. Med.* **72**(6), 1565–1579 (2014).
2. M. Engstrom and S. Skare, "Diffusion-weighted 3D multislab echo planar imaging for high signal-to-noise ratio efficiency and isotropic image resolution," *Magn. Reson. Med.* **70**(6), 1507–1514 (2013).
3. C. L. Johnson et al., "3D multislab, multishot acquisition for fast, whole-brain MR elastography with high signal-to-noise efficiency," *Magn. Reson. Med.* **71**(2), 477–485 (2014).
4. K. Setsompop et al., "Pushing the limits of in vivo diffusion MRI for the Human Connectome Project," *Neuroimage* **80**, 220–233 (2013).
5. J. E. Tanner and E. O. Stejskal, "Restricted self-diffusion of protons in colloidal systems by pulsed-gradient spin-echo method," *J. Chem. Phys.* **49**(4), 1768 (1968).
6. T. G. Reese et al., "Reduction of eddy-current-induced distortion in diffusion MRI using a twice-refocused spin echo," *Magn. Reson. Med.* **49**(1), 177–182 (2003).
7. J. L. Andersson and S. N. Sotiropoulos, "An integrated approach to correction for off-resonance effects and subject movement in diffusion MR imaging," *Neuroimage* **125**, 1063–1078 (2016).
8. N. G. Papadakis et al., "Gradient preemphasis calibration in diffusion-weighted echo-planar imaging," *Magn. Reson. Med.* **44**(4), 616–624 (2000).
9. J. Pipe, "Pulse Sequences for Diffusion-weighted MRI," in *Diffusion MRI: From Quantitative Measurement to In-vivo Neuroanatomy*, pp. 11–35 (2009).
10. G. J. Stanisz et al., "T1, T2 relaxation and magnetization transfer in tissue at 3T," *Magn. Reson. Med.* **54**(3), 507–512 (2005).
11. M. Engstrom et al., "On the signal-to-noise ratio efficiency and slab-banding artifacts in three-dimensional multislab diffusion-weighted echo-planar imaging," *Magn. Reson. Med.* **73**(2), 718–725 (2015).
12. R. Frost et al., "Scan time reduction for readout-segmented EPI using simultaneous multislice acceleration: diffusion-weighted imaging at 3 and 7 Tesla," *Magn. Reson. Med.* **74**(1), 136–149 (2015).
13. K. Setsompop et al., "Improving diffusion MRI using simultaneous multi-slice echo planar imaging," *NeuroImage* **63**(1), 569–580 (2012).
14. B. Zahneisen et al., "Three-dimensional Fourier encoding of simultaneously excited slices: generalized acquisition and reconstruction framework," *Magn. Reson. Med.* **71**(6), 2071–2081 (2014).
15. A. W. Anderson and J. C. Gore, "Analysis and correction of motion artifacts in diffusion weighted imaging," *Magn. Reson. Med.* **32**(3), 379–387 (1994).
16. Z. Zhang et al., "Self-feeding MUSE: a robust method for high resolution diffusion imaging using interleaved EPI," *NeuroImage* **105**, 552-560 (2015).

17. A. T. Van, D. Hernando, and B. P. Sutton, "Motion-induced phase error estimation and correction in 3D diffusion tensor imaging," *IEEE Trans. Med. Imaging* **30**(11), 1933–1940 (2011).
18. C. Liu et al., "Self-navigated interleaved spiral (SNAILS): application to high-resolution diffusion tensor imaging," *Magn. Reson. Med.* **52**(6), 1388–1396 (2004).
19. R. J. Ordidge et al., "Correction of motional artifacts in diffusion-weighted MR images using navigator echoes," *Magn. Reson. Imaging* **12**(3), 455–460 (1994).
20. D. Atkinson et al., "Sampling and reconstruction effects due to motion in diffusion-weighted interleaved echo planar imaging," *Magn. Reson. Med.* **44**(1), 101–109 (2000).
21. A. T. Van et al., "K-space and image space combination for motion artifact correction in multicoil multishot diffusion weighted imaging," in *Conf. Proc. IEEE Engineering Medical Biology Society*, pp. 1675–1678 (2008).
22. C. Liu, M. E. Moseley, and R. Bammer, "Simultaneous phase correction and SENSE reconstruction for navigated multi-shot DWI with non-cartesian k-space sampling," *Magn. Reson. Med.* **54**(6), 1412–1422 (2005).
23. T. K. Truong, N. K. Chen, and A. W. Song, "Inherent correction of motion-induced phase errors in multishot spiral diffusion-weighted imaging," *Magn. Reson. Med.* **68**(4), 1255–1261 (2012).
24. T. K. Truong and A. Guidon, "High-resolution multishot spiral diffusion tensor imaging with inherent correction of motion-induced phase errors," *Magn. Reson. Med.* **71**(2), 790–796 (2014).
25. J. Pauly et al., "Parameter relations for the Shinnar-Le Roux selective excitation pulse design algorithm [NMR imaging]," *IEEE Trans. Med. Imaging* **10**(1), 53–65 (1991).
26. K. P. Pruessmann et al., "SENSE: sensitivity encoding for fast MRI," *Magn. Reson. Med.* **42**(5), 952–962 (1999).
27. B. P. Sutton, D. C. Noll, and J. A. Fessler, "Fast, iterative image reconstruction for MRI in the presence of field inhomogeneities," *IEEE Trans. Med. Imaging* **22**(2), 178–188 (2003).
28. S. P. Sutton et al., "Faster dynamic imaging of speech with field inhomogeneity corrected spiral fast low angle shot (FLASH) at 3 T," *J. Magn. Reson. Imaging* **32**(5), 1228–1237 (2010).
29. J. A. Fessler, D. Yeo, and D. C. Noll, "Regularized fieldmap estimation in MRI," in *2006 3rd IEEE Int. Symp. on Biomedical Imaging: Macro to Nano*, Vols. 1–3, pp. 706–709 (2006).
30. Y. Zhang, M. Brady, and S. Smith, "Segmentation of brain MR images through a hidden Markov random field model and the expectation-maximization algorithm," *IEEE Trans. Med. Imaging* **20**(1), 45–57 (2001).
31. M. Jenkinson et al., "FSL," *Neuroimage* **62**(2), 782–790 (2012).
32. M. Jenkinson et al., "Improved optimization for the robust and accurate linear registration and motion correction of brain images," *NeuroImage* **17**(2), 825–841 (2002).
33. M. Jenkinson and S. Smith, "A global optimisation method for robust affine registration of brain images," *Med. Image Anal.* **5**(2), 143–156 (2001).
34. T. E. Behrens et al., "Characterization and propagation of uncertainty in diffusion-weighted MR imaging," *Magn. Reson. Med.* **50**(5), 1077–1088 (2003).
35. C. Lebel, T. Benner, and C. Beaulieu, "Six is enough? Comparison of diffusion parameters measured using six or more diffusion-encoding gradient directions with deterministic tractography," *Magn. Reson. Med.* **68**(2), 474–483 (2012).

**Joseph L. Holtrop** is currently pursing a PhD in bioengineering at the University of Illinois at Urbana-Champaign, working in the Magnetic Resonance Functional Imaging Lab. His research focuses on data acquisition approaches and model-based image reconstruction in MRI.

**Bradley P. Sutton** is an associate professor in the Bioengineering Department and the technical director of the Biomedical Imaging Center in the Beckman Institute at the University of Illinois at Urbana-Champaign. He received his PhD in biomedical engineering from the University of Michigan. His research interests include acquisition/image reconstruction approaches for neuroimaging.